

# STABILITY AND RESOLUTION ANALYSIS FOR A TOPOLOGICAL DERIVATIVE BASED IMAGING FUNCTIONAL\*

HABIB AMMARI<sup>†</sup>, JOSSELIN GARNIER<sup>‡</sup>, VINCENT JUGNON<sup>§</sup>, AND HYEONBAE  
KANG<sup>¶</sup>

**Abstract.** The aim of this paper is to study a topological derivative based anomaly detection algorithm. We compare its performance with other imaging approaches such as Multiple Signal Classification algorithm (MUSIC), backpropagation, and Kirchhoff migration. We also investigate its stability with respect to medium and measurement noises as well as its resolution. A simple postprocessing of the data set is introduced and shown to be essential in order to obtain an efficient topological based imaging functional, both in terms of resolution and stability.

**AMS subject classifications.** 35R30, 35B30

**Key words.** stability, resolution, imaging, Helmholtz equation, topological derivative, MUSIC, backpropagation, Kirchhoff migration, asymptotic expansion

**1. Problem Formulation.** Consider an acoustic anomaly with constant bulk modulus  $K$  and volumetric mass density  $\rho$ . The background medium  $\Omega$  is smooth and homogeneous with bulk modulus and density equal to one. Suppose that the operating frequency  $\omega$  is such that  $\omega^2$  is not an eigenvalue for the operator  $-\Delta$  in  $L^2(\Omega)$  with homogeneous Neumann boundary conditions. The scalar acoustic pressure  $u$  generated by the Neumann data  $g$  in the presence of the anomaly  $D$  is the solution to the Helmholtz equation:

$$\begin{cases} \nabla \cdot (\mathbf{1}_{\Omega \setminus \overline{D}}(\mathbf{x}) + \rho^{-1} \mathbf{1}_D(\mathbf{x})) \nabla u + \omega^2 (\mathbf{1}_{\Omega \setminus \overline{D}}(\mathbf{x}) + K^{-1} \mathbf{1}_D(\mathbf{x})) u = 0 & \text{in } \Omega, \\ \frac{\partial u}{\partial \nu} = g & \text{on } \partial\Omega, \end{cases} \quad (1.1)$$

while the background solution  $U$  satisfies

$$\begin{cases} \Delta U + \omega^2 U = 0 & \text{in } \Omega, \\ \frac{\partial U}{\partial \nu} = g & \text{on } \partial\Omega. \end{cases} \quad (1.2)$$

Here,  $\nu$  is the outward normal to  $\partial\Omega$  and  $\mathbf{1}_D$  is the characteristic function of  $D$ .

The problem under consideration is the following one: given the field  $u$  measured at the surface of the domain  $\Omega$ , we want to estimate the location of the anomaly  $D$ .

Recently, the concept of topological derivative has been applied in the imaging of small anomalies. See, for instance, [12, 13, 15, 9, 20, 17, 16]. The concept first appeared in shape optimization [14, 23, 11]. However, the use of the topological based imaging functional has been heuristic. As far as we know, it lacks mathematical justification. A stability and resolution investigation is also missing in the literature.

The goal of this paper is threefold: (i) to explain why the concept of topological derivative works for imaging small acoustic anomalies, (ii) to compare the topological derivative based imaging functional with other widely used imaging approaches such as Multiple Signal Classification (MUSIC), backpropagation, and Kirchhoff

---

\*This work was supported by National Institute for Mathematical Sciences (2010 Thematic Program, TP1003) and NRF grants No. 2009-0090250 and 2010-0017532.

<sup>†</sup>Department of Mathematics and Applications, Ecole Normale Supérieure, 45 Rue d'Ulm, 75005 Paris, France (habib.ammari@ens.fr).

<sup>‡</sup>Laboratoire de Probabilités et Modèles Aléatoires & Laboratoire Jacques-Louis Lions, Université Paris VII, 2 Place Jussieu, 75251 Paris Cedex 5, France (garnier@math.jussieu.fr).

<sup>§</sup>Centre de Mathématiques Appliquées, CNRS UMR 7641, Ecole Polytechnique, 91128 Palaiseau, France (jugnon@cmap.polytechnique.fr).

<sup>¶</sup>Department of Mathematics, Inha University, Incheon 402-751, Korea (hbkang@inha.ac.kr).

migration, and (iii) to carry out a detailed stability and resolution analysis for the topological derivative based algorithm. Both medium and measurement noises are considered.

The paper is organized as follows. In Section 2, we recall an asymptotic expansion of the boundary pressure perturbations. In Section 3, we introduce the topological derivative based imaging functional and prove that it attains its maximum at the location of the anomaly. Sections 4 and 5 are devoted to a stability and resolution analysis of the topological derivative based functional in the presence of medium and measurement noise, respectively. In Section 6, we review MUSIC, backpropagation, and Kirchhoff migration imaging approaches. In Section 7, we perform a variety of numerical tests to compare the topological derivative based imaging functional with MUSIC and backpropagation. The paper ends with a short discussion.

## 2. Asymptotic Analysis of the Boundary Pressure Perturbations.

Suppose that the anomaly is  $D = \mathbf{z}_a + \delta B$ , where  $\mathbf{z}_a$  is the ‘‘center’’ of  $D$ ,  $B$  is a smooth reference domain which contains the origin, and  $\delta$ , the characteristic size of  $D$ , is a small parameter.

In this section, we provide an asymptotic expansion of the boundary pressure perturbations,  $u - U$ , as  $\delta$  goes to zero. For doing so, we need to introduce a few auxiliary functions that can be computed either analytically or numerically.

For  $B$  a smooth bounded domain in  $\mathbb{R}^d$  and  $0 < k \neq 1 < +\infty$  a material parameter, let  $\hat{\mathbf{v}} = \hat{\mathbf{v}}(k, B)$  be the solution to

$$\begin{cases} \Delta \hat{\mathbf{v}} = \mathbf{0} & \text{in } \mathbb{R}^d \setminus \overline{B}, \\ \Delta \hat{\mathbf{v}} = \mathbf{0} & \text{in } B, \\ \hat{\mathbf{v}}|_- - \hat{\mathbf{v}}|_+ = \mathbf{0} & \text{on } \partial B, \\ k \frac{\partial \hat{\mathbf{v}}}{\partial \nu} \Big|_- - \frac{\partial \hat{\mathbf{v}}}{\partial \nu} \Big|_+ = \mathbf{0} & \text{on } \partial B, \\ \hat{\mathbf{v}}(\boldsymbol{\xi}) - \boldsymbol{\xi} \rightarrow \mathbf{0} & \text{as } |\boldsymbol{\xi}| \rightarrow +\infty. \end{cases} \quad (2.1)$$

Here we denote

$$v|_{\pm}(\boldsymbol{\xi}) := \lim_{t \rightarrow 0^+} v(\boldsymbol{\xi} \pm t\nu_{\boldsymbol{\xi}}), \quad \boldsymbol{\xi} \in \partial B,$$

and

$$\frac{\partial v}{\partial \nu} \Big|_{\pm}(\boldsymbol{\xi}) := \lim_{t \rightarrow 0^+} \nu_{\boldsymbol{\xi}}^T \nabla v(\boldsymbol{\xi} \pm t\nu_{\boldsymbol{\xi}}), \quad \boldsymbol{\xi} \in \partial B,$$

if the limits exist, where  $\nu_{\boldsymbol{\xi}}$  is the outward unit normal to  $\partial B$  at  $\boldsymbol{\xi}$  and  $T$  stands for the transpose (so that  $\mathbf{a}^T \mathbf{b}$  is the scalar product of the two vectors  $\mathbf{a}$  and  $\mathbf{b}$ ). Recall that  $\hat{\mathbf{v}}$  plays the role of the first-order corrector in the theory of homogenization [21].

Define the polarization tensor  $\mathbf{M}(k, B) = (M_{pq})_{p,q=1}^d$  by

$$M_{pq}(k, B) := (k - 1) \int_B \frac{\partial \hat{v}_q}{\partial \xi_p}(\boldsymbol{\xi}) d\boldsymbol{\xi}, \quad (2.2)$$

where  $\hat{\mathbf{v}} = (\hat{v}_1, \dots, \hat{v}_d)^T$  is the solution to (2.1). The formula of the polarization tensor for ellipses will be useful. Let  $B$  be an ellipse whose semi-axes are along the  $x_1$ - and  $x_2$ -axes and of length  $a$  and  $b$ , respectively. Then,  $\mathbf{M}(k, B)$  takes the form

$$\mathbf{M}(k, B) = (k - 1)|B| \begin{pmatrix} \frac{a+b}{a+kb} & 0 \\ 0 & \frac{a+b}{b+ka} \end{pmatrix}. \quad (2.3)$$

For  $\omega \geq 0$ , let for  $\mathbf{x} \neq 0$ ,

$$\Gamma_\omega(\mathbf{x}) = \begin{cases} \frac{e^{i\omega|\mathbf{x}|}}{4\pi|\mathbf{x}|}, & d = 3, \\ \frac{i}{4}H_0^{(1)}(\omega|\mathbf{x}|), & d = 2, \end{cases} \quad (2.4)$$

which is the outgoing fundamental solution for the Helmholtz operator  $-(\Delta + \omega^2)$  in  $\mathbb{R}^d$ . Here,  $H_0^{(1)}$  is the Hankel function of the first kind of order zero.

Let  $\mathcal{S}_\Omega^\omega$  be the single-layer potential for  $\Delta + \omega^2$ , that is,

$$\mathcal{S}_\Omega^\omega[\varphi](\mathbf{x}) = \int_{\partial\Omega} \Gamma_\omega(\mathbf{x} - \mathbf{y})\varphi(\mathbf{y}) d\sigma(\mathbf{y}), \quad \mathbf{x} \in \mathbb{R}^d, \quad (2.5)$$

for  $\varphi \in L^2(\partial\Omega)$ . Let the integral operator  $\mathcal{K}_\Omega^\omega$  be defined by

$$\mathcal{K}_\Omega^\omega[\varphi](\mathbf{x}) = \int_{\partial\Omega} \frac{\partial\Gamma_\omega(\mathbf{x} - \mathbf{y})}{\partial\nu(\mathbf{y})}\varphi(\mathbf{y})d\sigma(\mathbf{y}), \quad \mathbf{x} \in \partial\Omega.$$

It is well-known that the normal derivative of  $\mathcal{S}_\Omega^\omega$  obeys the following jump relation [5]:

$$\frac{\partial(\mathcal{S}_\Omega^\omega[\varphi])}{\partial\nu} \Big|_{\pm}(\mathbf{x}) = \left( \pm \frac{1}{2}\mathcal{I} + (\mathcal{K}_\Omega^{-\omega})^* \right)[\varphi](\mathbf{x}) \quad \text{a.e. } \mathbf{x} \in \partial\Omega, \quad (2.6)$$

for  $\varphi \in L^2(\partial\Omega)$ , where  $(\mathcal{K}_\Omega^{-\omega})^*$  is the  $L^2$ -adjoint of  $\mathcal{K}_\Omega^{-\omega}$ ; that is,

$$(\mathcal{K}_\Omega^{-\omega})^*[\varphi](\mathbf{x}) = \int_{\partial\Omega} \frac{\partial\Gamma_\omega(\mathbf{x} - \mathbf{y})}{\partial\nu(\mathbf{x})}\varphi(\mathbf{y})d\sigma(\mathbf{y}).$$

For  $\mathbf{z} \in \Omega$ , let us now introduce the Neumann function for  $-(\Delta + \omega^2)$  in  $\Omega$  corresponding to a Dirac mass at  $\mathbf{z}$ . That is,  $N_\omega$  is the solution to

$$\begin{cases} -(\Delta_x + \omega^2)N_\omega(\mathbf{x}, \mathbf{z}) = \delta_{\mathbf{z}} & \text{in } \Omega, \\ \frac{\partial N_\omega}{\partial\nu} = 0 & \text{on } \partial\Omega. \end{cases} \quad (2.7)$$

We will need the following lemma from [7, Proposition 2.8].

LEMMA 2.1. *The following identity relating the fundamental solution  $\Gamma_\omega$  to the Neumann function  $N_\omega$  holds:*

$$\left( -\frac{1}{2}\mathcal{I} + \mathcal{K}_\Omega^\omega \right)[N_\omega(\cdot, \mathbf{z})](\mathbf{x}) = \Gamma_\omega(\mathbf{x} - \mathbf{z}), \quad \mathbf{x} \in \partial\Omega, \quad \mathbf{z} \in \Omega. \quad (2.8)$$

In (2.8),  $\mathcal{I}$  denotes the identity. Assuming that  $\omega^2$  is not an eigenvalue for the operator  $-\Delta$  in  $L^2(\Omega)$  with homogeneous Neumann boundary conditions, we can prove, using the theory of relatively compact operators, the existence and uniqueness of a solution to (1.1) at least for  $\delta$  small enough [24]. Moreover, the following asymptotic formula for boundary pressure perturbations that are due to the presence of a small acoustic anomaly holds [24, 5].

THEOREM 2.2. *Let  $u$  be the solution of (1.1) and let  $U$  be the background solution. Suppose that  $D = \mathbf{z}_a + \delta B$ , with  $0 < (K, \rho) \neq (1, 1) < +\infty$ . Suppose that  $\omega\delta \ll 1$ .*

(i) *For any  $\mathbf{x} \in \partial\Omega$ ,*

$$u(\mathbf{x}) = U(\mathbf{x}) - \delta^d \left( \nabla U(\mathbf{z}_a)^T \mathbf{M}(1/\rho, B) \nabla_{\mathbf{z}} N_\omega(\mathbf{x}, \mathbf{z}_a) + \omega^2 (K^{-1} - 1) |B| U(\mathbf{z}) N_\omega(\mathbf{x}, \mathbf{z}_a) \right) + o(\delta^d), \quad (2.9)$$

where  $\mathbf{M}(1/\rho, B)$  is the polarization tensor associated with  $B$  and  $1/\rho$ .

(ii) Let  $w$  be a smooth function such that  $(\Delta + \omega^2)w = 0$  in  $\Omega$ . The weighted boundary measurements  $I_w[U, \omega]$  defined by

$$I_w[U, \omega] := \int_{\partial\Omega} (u - U)(\mathbf{x}) \frac{\partial w}{\partial \nu}(\mathbf{x}) d\sigma(\mathbf{x}) \quad (2.10)$$

satisfies

$$I_w[U, \omega] \simeq -\delta^d \left( \nabla U(\mathbf{z}_a)^T \mathbf{M}(1/\rho, B) \nabla w(\mathbf{z}_a) + \omega^2 (K^{-1} - 1) |B| U(\mathbf{z}_a) w(\mathbf{z}_a) \right). \quad (2.11)$$

Combining (2.9) and Lemma 2.1, the following corollary immediately holds.

COROLLARY 2.3. For any  $\mathbf{x} \in \partial\Omega$ ,

$$\begin{aligned} \left(-\frac{1}{2}\mathcal{I} + \mathcal{K}_\Omega^\omega\right)[u - U](\mathbf{x}) &= -\delta^d \left( \nabla U(\mathbf{z}_a)^T \mathbf{M}(1/\rho, B) \nabla_z \Gamma_\omega(\mathbf{x} - \mathbf{z}_a) \right. \\ &\quad \left. + \omega^2 (K^{-1} - 1) |B| U(\mathbf{z}_a) \Gamma_\omega(\mathbf{x} - \mathbf{z}_a) \right) + o(\delta^d). \end{aligned} \quad (2.12)$$

**3. Topological Derivative Based Imaging Functional.** Suppose that  $K > 1$  and  $\rho > 1$  (one of the two inequalities could be an equality). To locate the anomaly  $D$ , we consider the quadratic misfit

$$\mathcal{E}[U](\mathbf{z}^S) = \frac{1}{2} \int_{\partial\Omega} \left| \left(-\frac{1}{2}\mathcal{I} + \mathcal{K}_\Omega^\omega\right)[u_{\mathbf{z}^S} - u_{\text{meas}}](\mathbf{x}) \right|^2 d\sigma(\mathbf{x}) \quad (3.1)$$

over the search points  $\mathbf{z}^S$ , where  $u_{\mathbf{z}^S}$  is the solution of (1.1) with  $D' = \mathbf{z}^S + \delta' B'$ ,  $K' > 1$ ,  $\rho' > 1$ ,  $B'$  being chosen a priori, and  $\delta'$  being small. If  $K < 1$  and  $\rho < 1$ , then we choose  $K' < 1$  and  $\rho' < 1$ . According to Theorem 2.2, the synthetic field  $u_{\mathbf{z}^S}$  can be expanded with respect to  $\delta'$  as

$$\begin{aligned} u_{\mathbf{z}^S}(\mathbf{x}) &= U(\mathbf{x}) - (\delta')^d \left( \nabla U(\mathbf{z}^S)^T \mathbf{M}(1/\rho', B') \nabla_z N_\omega(\mathbf{x}, \mathbf{z}^S) \right. \\ &\quad \left. + \omega^2 (K'^{-1} - 1) |B'| U(\mathbf{z}^S) N_\omega(\mathbf{x}, \mathbf{z}^S) \right) + o((\delta')^d). \end{aligned}$$

Therefore, in view of Corollary 2.3, the quadratic misfit function can be expanded as powers of  $\delta'$  as

$$\begin{aligned} \mathcal{E}[U](\mathbf{z}^S) &= \frac{1}{2} \int_{\partial\Omega} \left| \left(-\frac{1}{2}\mathcal{I} + \mathcal{K}_\Omega^\omega\right)[u_{\mathbf{z}^S} - U + U - u_{\text{meas}}](\mathbf{x}) \right|^2 d\sigma(\mathbf{x}) \\ &= \frac{1}{2} \int_{\partial\Omega} \left| \left(-\frac{1}{2}\mathcal{I} + \mathcal{K}_\Omega^\omega\right)[U - u_{\text{meas}}](\mathbf{x}) \right|^2 d\sigma(\mathbf{x}) \\ &\quad - (\delta')^d \operatorname{Re} \left\{ \nabla U(\mathbf{z}^S)^T \mathbf{M}(1/\rho', B') \int_{\partial\Omega} \nabla_z \Gamma_\omega(\mathbf{x} - \mathbf{z}^S) \overline{\left(-\frac{1}{2}\mathcal{I} + \mathcal{K}_\Omega^\omega\right)[U - u_{\text{meas}}](\mathbf{x})} d\sigma(\mathbf{x}) \right\} \\ &\quad - (\delta')^d \omega^2 (K'^{-1} - 1) |B'| \operatorname{Re} \left\{ U(\mathbf{z}^S) \int_{\partial\Omega} \Gamma_\omega(\mathbf{x} - \mathbf{z}^S) \overline{\left(-\frac{1}{2}\mathcal{I} + \mathcal{K}_\Omega^\omega\right)[U - u_{\text{meas}}](\mathbf{x})} d\sigma(\mathbf{x}) \right\} \\ &\quad + o((\delta\delta')^d + (\delta')^{2d}). \end{aligned}$$

Let  $w$  be defined in terms of  $u_{\text{meas}} - U$  as

$$w(\mathbf{x}) = \mathcal{S}_\Omega^\omega \overline{\left(-\frac{1}{2}\mathcal{I} + \mathcal{K}_\Omega^\omega\right)[U - u_{\text{meas}}](\mathbf{x})} \quad \text{for } \mathbf{x} \in \Omega, \quad (3.2)$$

where  $\mathcal{S}_\Omega^\omega$  is defined by (2.5). From (2.6), it follows that  $w$  is the solution of the Helmholtz equation

$$\begin{cases} \Delta w + \omega^2 w = 0 & \text{in } \Omega, \\ \frac{\partial w}{\partial \nu} = \left(-\frac{1}{2}\mathcal{I} + (\mathcal{K}_\Omega^{-\omega})^*\right) \overline{\left(-\frac{1}{2}\mathcal{I} + \mathcal{K}_\Omega^\omega\right)[U - u_{\text{meas}}]} & \text{on } \partial\Omega. \end{cases} \quad (3.3)$$

The function  $w$  is obtained by backpropagating the Neumann data

$$\left(-\frac{1}{2}\mathcal{I} + (\mathcal{K}_\Omega^\omega)^*\right)\left(-\frac{1}{2}\mathcal{I} + \mathcal{K}_\Omega^\omega\right)[U - u_{\text{meas}}]$$

inside the background medium (without any anomaly). Note that  $\overline{(\mathcal{K}_\Omega^\omega)^*} = (\mathcal{K}_\Omega^{-\omega})^*$ .

Therefore, we can rewrite the expansion of the quadratic misfit function as

$$\begin{aligned} \mathcal{E}[U](\mathbf{z}^S) &= \frac{1}{2} \int_{\partial\Omega} \left| \left(-\frac{1}{2}\mathcal{I} + \mathcal{K}_\Omega^\omega\right)[U - u_{\text{meas}}](\mathbf{x}) \right|^2 d\sigma(\mathbf{x}) \\ &\quad - (\delta')^d \text{Re} \left\{ \nabla U(\mathbf{z}^S)^T \mathbf{M}(1/\rho', B') \nabla w(\mathbf{z}^S) + \omega^2 (K'^{-1} - 1) |B'| U(\mathbf{z}^S) w(\mathbf{z}^S) \right\} \\ &\quad + o((\delta\delta')^d + (\delta')^{2d}). \end{aligned}$$

By computing the topological derivative for  $\mathbf{z}^S \in \Omega$ ,

$$\mathcal{I}_{\text{TD}}[U](\mathbf{z}^S) := - \left. \frac{\partial \mathcal{E}[U]}{\partial (\delta')^d} \right|_{(\delta')^d=0},$$

*i.e.*, minus the derivative of  $\mathcal{E}[U]$  with respect to the volume  $(\delta')^d$  at zero, we obtain the values of the topological derivative imaging functional:

$$\mathcal{I}_{\text{TD}}[U](\mathbf{z}^S) = \text{Re} \left\{ \nabla U(\mathbf{z}^S)^T \mathbf{M}(1/\rho', B') \nabla w(\mathbf{z}^S) + \omega^2 (K'^{-1} - 1) |B'| U(\mathbf{z}^S) w(\mathbf{z}^S) \right\}. \quad (3.4)$$

The functional  $\mathcal{I}_{\text{TD}}[U](\mathbf{z}^S)$  gives, at every search point  $\mathbf{z}^S \in \Omega$ , the sensitivity of the misfit function relative to the insertion of an anomaly  $D' = \mathbf{z}^S + \delta' B'$  at the point  $\mathbf{z}^S$ . The maximum of  $\mathcal{I}_{\text{TD}}[U](\mathbf{z}^S)$  corresponds to the point at which the insertion of an anomaly centered at that point maximally decreases the misfit function. The location of the maximum of  $\mathcal{I}_{\text{TD}}[U](\mathbf{z}^S)$  is, therefore, a good estimate of the location  $\mathbf{z}_a$  of the anomaly that determines the measured field  $u_{\text{meas}}$ . In fact, as we show below the functional  $\mathcal{I}_{\text{TD}}$  attains its maximum at  $\mathbf{z}^S = \mathbf{z}_a$ .

Substituting (2.9) into (3.2), we find that

$$\begin{aligned} w(\mathbf{z}^S) &= \delta^d \left( \nabla \overline{U}(\mathbf{z}_a)^T \mathbf{M}(1/\rho, B) \int_{\partial\Omega} \nabla_{\mathbf{z}} \overline{\Gamma}_\omega(\mathbf{x} - \mathbf{z}_a) \nabla \Gamma_\omega(\mathbf{x} - \mathbf{z}^S) d\sigma(\mathbf{x}) \right. \\ &\quad \left. + \omega^2 (K^{-1} - 1) \overline{U}(\mathbf{z}_a) \int_{\partial\Omega} \overline{\Gamma}_\omega(\mathbf{x} - \mathbf{z}_a) \Gamma_\omega(\mathbf{x} - \mathbf{z}^S) d\sigma(\mathbf{x}) \right) + o(\delta^d), \end{aligned}$$

and, for  $j = 1, \dots, d$ ,

$$\begin{aligned} \frac{\partial w(\mathbf{z}^S)}{\partial z_j^S} &= \delta^d \left( \nabla \overline{U}(\mathbf{z}_a)^T \mathbf{M}(1/\rho, B) \int_{\partial\Omega} \nabla_{\mathbf{z}} \overline{\Gamma}_\omega(\mathbf{x} - \mathbf{z}_a) \frac{\partial \Gamma_\omega(\mathbf{x} - \mathbf{z}^S)}{\partial z_j^S} d\sigma(\mathbf{x}) \right. \\ &\quad \left. + \omega^2 (K^{-1} - 1) \overline{U}(\mathbf{z}_a) \int_{\partial\Omega} \overline{\Gamma}_\omega(\mathbf{x} - \mathbf{z}_a) \frac{\partial \Gamma_\omega(\mathbf{x} - \mathbf{z}^S)}{\partial z_j^S} d\sigma(\mathbf{x}) \right) + o(\delta^d). \end{aligned}$$

We now explain in more detail why the topological derivative imaging functional attains its highest value at the location  $\mathbf{z}_a$  of the anomaly. For simplicity assume that  $K = 1$  or  $\rho = 1$ .

If  $\rho = 1$  then

$$\begin{aligned} \mathcal{I}_{\text{TD}}[U](\mathbf{z}^S) &= \delta^d \omega^4 (K'^{-1} - 1) (K^{-1} - 1) |B'| \text{Re} \left\{ U(\mathbf{z}^S) r_\omega(\mathbf{z}^S, \mathbf{z}_a) \overline{U}(\mathbf{z}_a) \right\} \\ &\quad + o(\delta^d), \end{aligned} \quad (3.5)$$

$$r_\omega(\mathbf{z}^S, \mathbf{z}) := \int_{\partial\Omega} \Gamma_\omega(\mathbf{x} - \mathbf{z}^S) \overline{\Gamma}_\omega(\mathbf{x} - \mathbf{z}) d\sigma(\mathbf{x}). \quad (3.6)$$

If  $K = 1$  then

$$\begin{aligned} \mathcal{I}_{\text{TD}}[U](\mathbf{z}^S) &= \delta^d \operatorname{Re} \left\{ \nabla U(\mathbf{z}^S)^T \mathbf{M}(1/\rho', B') \mathbf{R}_\omega(\mathbf{z}^S, \mathbf{z}_a) \mathbf{M}(1/\rho, B)^T \nabla \overline{U}(\mathbf{z}_a) \right\} \\ &\quad + o(\delta^d), \\ \mathbf{R}_\omega(\mathbf{z}^S, \mathbf{z}) &:= \int_{\partial\Omega} \nabla_{\mathbf{z}} \Gamma_\omega(\mathbf{x} - \mathbf{z}^S) \nabla_{\mathbf{z}} \overline{\Gamma_\omega}(\mathbf{x} - \mathbf{z})^T d\sigma(\mathbf{x}). \end{aligned}$$

Recall that Helmholtz-Kirchhoff theorem (see, *e.g.*, [1]) states that, for  $\mathbf{z}$  and  $\mathbf{z}^S$  away from the boundary  $\partial\Omega$ , the quantities  $r_\omega(\mathbf{z}^S, \mathbf{z})$  and  $\mathbf{R}_\omega(\mathbf{z}^S, \mathbf{z})$  are (approximately) proportional to the imaginary part of  $\Gamma_\omega$ :

$$\begin{aligned} \int_{\partial\Omega} \overline{\Gamma_\omega}(\mathbf{x} - \mathbf{z}) \Gamma_\omega(\mathbf{x} - \mathbf{z}^S) d\sigma(\mathbf{x}) &\sim \frac{1}{\omega} \operatorname{Im} \{ \Gamma_\omega(\mathbf{z}^S - \mathbf{z}) \}, \\ \int_{\partial\Omega} \nabla_{\mathbf{z}} \Gamma_\omega(\mathbf{x} - \mathbf{z}^S) \nabla_{\mathbf{z}} \overline{\Gamma_\omega}(\mathbf{x} - \mathbf{z})^T d\sigma(\mathbf{x}) &\sim \omega \operatorname{Im} \{ \Gamma_\omega(\mathbf{z}^S - \mathbf{z}) \} \left( \frac{\mathbf{z} - \mathbf{z}^S}{|\mathbf{z} - \mathbf{z}^S|} \right) \left( \frac{\mathbf{z} - \mathbf{z}^S}{|\mathbf{z} - \mathbf{z}^S|} \right)^T. \end{aligned}$$

Here,  $A \sim B$  means  $A \simeq CB$  for some constant  $C$ .

Let, for simplicity,  $(\boldsymbol{\theta}_1, \dots, \boldsymbol{\theta}_n)$  be  $n$  equi-distributed directions on the unit sphere and denote by  $U_j$  the plane wave

$$U_j(\mathbf{x}) = e^{i\omega \boldsymbol{\theta}_j^T \mathbf{x}}, \quad \mathbf{x} \in \Omega, \quad j = 1, \dots, n. \quad (3.7)$$

For sufficiently large  $n$  we have

$$\frac{1}{n} \sum_{l=1}^n e^{i\omega \boldsymbol{\theta}_l^T \mathbf{x}} \simeq 4 \left( \frac{\pi}{\omega} \right)^{d-2} \operatorname{Im} \{ \Gamma_\omega(\mathbf{x}) \} = \begin{cases} \operatorname{sinc}(\omega|\mathbf{x}|) & \text{for } d = 3, \\ J_0(\omega|\mathbf{x}|) & \text{for } d = 2, \end{cases} \quad (3.8)$$

where  $\operatorname{sinc}(s) = \sin(s)/s$  is the sinc function and  $J_0$  is the Bessel function of the first kind and of order zero.

When  $\rho = 1$ , by computing the topological derivatives for the  $n$  plane waves, we obtain

$$\begin{aligned} \frac{1}{n} \sum_{j=1}^n \mathcal{I}_{\text{TD}}[U_j](\mathbf{z}^S) &\simeq \frac{\delta^d \omega^4}{n} \sum_{j=1}^n \operatorname{Re} \{ e^{i\omega \boldsymbol{\theta}_j^T (\mathbf{z}^S - \mathbf{z}_a)} r_\omega(\mathbf{z}^S, \mathbf{z}_a) \} \\ &\sim \omega^{5-d} (\operatorname{Im} \{ \Gamma_\omega(\mathbf{z}^S - \mathbf{z}_a) \})^2. \end{aligned} \quad (3.9)$$

Similarly, when  $K = 1$ , by computing the topological derivatives for the  $n$  plane waves,  $U_j, j = 1, \dots, n$ , given by (3.7), we obtain

$$\frac{1}{n} \sum_{j=1}^n \mathcal{I}_{\text{TD}}[U_j](\mathbf{z}^S) \simeq \delta^d \omega^2 \frac{1}{n} \sum_{j=1}^n \operatorname{Re} \{ e^{i\omega \boldsymbol{\theta}_j^T (\mathbf{z}^S - \mathbf{z}_a)} [\boldsymbol{\theta}_j^T \mathbf{M}(1/\rho', B') \mathbf{R}_\omega(\mathbf{z}^S, \mathbf{z}_a) \mathbf{M}(1/\rho, B)^T \boldsymbol{\theta}_j] \}.$$

Using  $\rho' = 0$  and  $B'$  the unit disk, the polarization tensor  $\mathbf{M}(1/\rho', B') = C_d \mathbf{I}$ , where  $C_d$  is a constant, is proportional to the identity. If, additionally, we assume that  $\mathbf{M}(1/\rho, B)$  is approximately proportional to the identity, which occurs in particular when  $B$  is a disk or a ball, then

$$\frac{1}{n} \sum_{j=1}^n \mathcal{I}_{\text{TD}}[U_j](\mathbf{z}^S) \sim \omega^{5-d} (\operatorname{Im} \{ \Gamma_\omega(\mathbf{z}^S - \mathbf{z}_a) \})^2. \quad (3.10)$$

Therefore, the topological derivative based imaging functional

$$\mathcal{I}_{\text{TD}}(\mathbf{z}^S) := \frac{1}{n} \sum_{j=1}^n \mathcal{I}_{\text{TD}}[U_j](\mathbf{z}^S) \quad (3.11)$$

attains its maximum at  $\mathbf{z}_a$ . Moreover, the resolution for the location estimation is given by the diffraction limit. It is of the order of half the wavelength  $\lambda = 2\pi/\omega$ .

We conclude this section by making a few remarks:

- In (3.1), we postprocess  $u_{\mathbf{z}} - u_{\text{meas}}$  by applying the integral operator  $(-\frac{1}{2}\mathcal{I} + \mathcal{K}_{\Omega}^{\omega})$ . This postprocessing is essential in order to derive an efficient topological based imaging functional. See Section 7.
- The topological derivative based imaging functional cannot detect anomalies close to the boundary.
- The results of this section apply to the Dirichlet problem as well as to the case of a hard anomaly.

#### 4. Stability with Respect to Medium Noise.

##### 4.1. The Topological Derivative in the Presence of Medium Noise.

We consider the case in which the medium is randomly heterogeneous around a constant background. Let  $K$  be the bulk modulus of the anomaly  $D$ . We assume that the density  $\rho$  of the anomaly is equal to one (*i.e.*, the same as the density of the background) in order to simplify the analysis, but the results could be extended to the general case in which  $\rho \neq 1$ . The scalar acoustic pressure  $u$  generated by the Neumann data  $g$  in the presence of the anomaly  $D$  is the solution to the Helmholtz equation:

$$\begin{cases} \Delta u + \omega^2 n^2(\mathbf{x})u = 0 & \text{in } \Omega, \\ \frac{\partial u}{\partial \nu} = g & \text{on } \partial\Omega. \end{cases} \quad (4.1)$$

The index of refraction is of the form

$$n^2(\mathbf{x}) = 1 + (K^{-1} - 1)\mathbf{1}_D(\mathbf{x}) + \mu(\mathbf{x}),$$

where 1 stands for the constant background,  $(K^{-1} - 1)\mathbf{1}_D(\mathbf{x})$  stands for the localized perturbation of the index of refraction due to the anomaly, and  $\mu(\mathbf{x})$  stands for the fluctuations of the index of refraction due to clutter. We assume that  $\mu$  is a random process with Gaussian statistics and mean zero, and that it is compactly supported within  $\Omega$ . The background solution  $U$ , *i.e.*, the field that would be observed without the anomaly, satisfies

$$\begin{cases} \Delta U + \omega^2(1 + \mu)U = 0 & \text{in } \Omega, \\ \frac{\partial U}{\partial \nu} = g & \text{on } \partial\Omega. \end{cases} \quad (4.2)$$

Note that  $U$  is not known because it depends on  $\mu$ , only the background reference solution  $U^{(0)}$  can be computed:

$$\begin{cases} \Delta U^{(0)} + \omega^2 U^{(0)} = 0 & \text{in } \Omega, \\ \frac{\partial U^{(0)}}{\partial \nu} = g & \text{on } \partial\Omega. \end{cases} \quad (4.3)$$

If the anomaly is of the form  $D = \mathbf{z}_a + \delta B$ , then one can show that the field measured at the surface of  $\Omega$  can be expanded as

$$u_{\text{meas}}(\mathbf{x}) = U(\mathbf{x}) - \delta^d \omega^2 (K^{-1} - 1) |B| U(\mathbf{z}_a) N_{\omega}(\mathbf{x}, \mathbf{z}_a) + o(\delta^d), \quad (4.4)$$

where  $N_{\omega}$  is the unknown Neumann function for  $-(\Delta + \omega^2(1 + \mu))$  (it is unknown because it depends on  $\mu$ ). It is worth mentioning that we changed the notation in this section:  $N_{\omega}$  is the Neumann function for  $-(\Delta + \omega^2(1 + \mu))$ , not for  $-(\Delta + \omega^2)$  as in the previous section. The Neumann function for  $-(\Delta + \omega^2)$  will be denoted by  $N_{\omega}^{(0)}$  (the superscript (0) indicates the ‘zero noise’).

We want to compare the measured data with the synthetic field  $u_{\mathbf{z}^S}$ , which is the solution of

$$\begin{cases} \Delta u_{\mathbf{z}^S} + \omega^2(1 + (K'^{-1} - 1)\mathbf{1}_{D'}(\mathbf{x}))u_{\mathbf{z}^S} = 0 & \text{in } \Omega, \\ \frac{\partial u_{\mathbf{z}^S}}{\partial \nu} = g & \text{on } \partial\Omega, \end{cases}$$

with  $D' = \mathbf{z}^S + \delta' B'$ ,  $K'$  and  $B'$  being chosen a priori, and  $\delta'$  being a small parameter. We can expand the synthetic field  $u_{\mathbf{z}^S}$  in powers of  $\delta'$  and we find that

$$u_{\mathbf{z}^S}(\mathbf{x}) = U^{(0)}(\mathbf{x}) - (\delta')^d \omega^2 (K'^{-1} - 1) |B'| U^{(0)}(\mathbf{z}^S) N_\omega^{(0)}(\mathbf{x}, \mathbf{z}^S) + o((\delta')^d).$$

The quadratic misfit functional

$$\mathcal{E}[U^{(0)}](\mathbf{z}^S) = \frac{1}{2} \int_{\partial\Omega} |(-\frac{1}{2}\mathcal{I} + \mathcal{K}_\Omega^{\omega, (0)})[u_{\mathbf{z}^S} - u_{\text{meas}}](\mathbf{x})|^2 d\sigma(\mathbf{x})$$

uses the background reference solution  $U^{(0)}$  and the known integral operator  $\mathcal{K}_\Omega^{\omega, (0)}$  defined in terms of the Green function  $\Gamma_\omega$  of the reference background medium. It can be expanded as powers of  $\delta'$  as

$$\begin{aligned} \mathcal{E}[U^{(0)}](\mathbf{z}^S) &= \frac{1}{2} \int_{\partial\Omega} |(-\frac{1}{2}\mathcal{I} + \mathcal{K}_\Omega^{\omega, (0)})[U^{(0)} - u_{\text{meas}}](\mathbf{x})|^2 d\sigma(\mathbf{x}) \\ &- (\delta')^d \omega^2 (K'^{-1} - 1) |B'| \text{Re} \left\{ U^{(0)}(\mathbf{z}^S) \int_{\partial\Omega} \overline{\Gamma_\omega(\mathbf{x} - \mathbf{z}^S) ((-\frac{1}{2}\mathcal{I} + \mathcal{K}_\Omega^{\omega, (0)})[U^{(0)} - u_{\text{meas}}](\mathbf{x}))} d\sigma(\mathbf{x}) \right\} \\ &+ o((\delta\delta')^d + (\delta')^{2d}), \end{aligned}$$

This shows that the computation of the topological derivative gives the imaging functional

$$\mathcal{I}_{\text{TD}}[U^{(0)}](\mathbf{z}^S) = \omega^2 (K'^{-1} - 1) |B'| \text{Re} \{ U^{(0)}(\mathbf{z}^S) w^{(0)}(\mathbf{z}^S) \}, \quad (4.5)$$

where  $w^{(0)}$  is given by

$$w^{(0)}(\mathbf{z}^S) = \mathcal{S}_\Omega^{\omega, (0)} \overline{((-\frac{1}{2}\mathcal{I} + \mathcal{K}_\Omega^{\omega, (0)})[U^{(0)} - u_{\text{meas}}])}(\mathbf{z}^S), \quad (4.6)$$

which is the known solution of

$$\begin{cases} \Delta w^{(0)} + \omega^2 w^{(0)} = 0 & \text{in } \Omega, \\ \frac{\partial w^{(0)}}{\partial \nu} = (-\frac{1}{2}\mathcal{I} + (\mathcal{K}_\Omega^{-\omega, (0)})^*) \overline{((-\frac{1}{2}\mathcal{I} + \mathcal{K}_\Omega^{\omega, (0)})[U^{(0)} - u_{\text{meas}}])} & \text{on } \partial\Omega. \end{cases}$$

Here,  $\mathcal{S}_\Omega^{\omega, (0)}$  is the single-layer potential associated with the Green function  $\Gamma_\omega$  of the reference background medium. The function  $w^{(0)}$  is known because it depends only on  $U^{(0)}$  that can be computed and on  $u_{\text{meas}}$  that is measured at the boundary.

**4.2. Stability and Resolution Analysis.** Let  $\Lambda^{(0)} = (-\frac{1}{2}\mathcal{I} + \mathcal{K}_\Omega^{\omega, (0)})^* (-\frac{1}{2}\mathcal{I} + \mathcal{K}_\Omega^{\omega, (0)})$ . We want now to carry out a resolution and stability analysis. Using (4.4) we have

$$\begin{aligned} w^{(0)}(\mathbf{z}^S) &= \int_{\partial\Omega} N_\omega^{(0)}(\mathbf{x}, \mathbf{z}^S) \overline{\Lambda^{(0)}[U^{(0)} - U]}(\mathbf{x}) d\sigma(\mathbf{x}) \\ &+ \delta^d \omega^2 (K^{-1} - 1) |B| \overline{U(\mathbf{z}_a)} \int_{\partial\Omega} \Lambda^{(0)}[N_\omega^{(0)}(\cdot, \mathbf{z}^S)](\mathbf{x}) \overline{N_\omega(\mathbf{x}, \mathbf{z}_a)} d\sigma(\mathbf{x}) \\ &+ o(\delta^d). \end{aligned} \quad (4.7)$$

This expression shows that clutter noise has two effects:

- First the background field  $U$  is not known, so that the backpropagation step transports not only the field due to the anomaly but also the field  $U - U^{(0)}$  due to clutter, which generates a contribution (the first term of the right-hand side of (4.7)) which is spatially distributed for  $\mathbf{z}^S$  throughout the domain  $\Omega$ .
- Second the Neumann function  $N_\omega$  is not known exactly, so that the backpropagation by  $N_\omega^{(0)}$  of the field generated by the anomaly is not perfect and may alter the sharp peak around  $\mathbf{z}^S \sim \mathbf{z}_a$  that is observed when the two Neumann functions are identical.

In the sequel we study the imaging functional in the weak fluctuation regime (when the standard deviation of  $\mu$  is small). For this we need to characterize the statistical distribution of the function  $w^{(0)}$  defined by (4.7):

- The first term of the right-hand side of (4.7) requires to model the difference  $U - U^{(0)}$ . If we assume that the random process  $\mu$  has small amplitude, then we can expand  $U$  as  $U = U^{(0)} + U^{(1)}$  where  $U^{(1)}$  is the solution of

$$\begin{cases} \Delta U^{(1)} + \omega^2 U^{(1)} = -\omega^2 \mu U^{(0)} & \text{in } \Omega, \\ \frac{\partial U^{(1)}}{\partial \nu} = 0 & \text{on } \partial\Omega. \end{cases} \quad (4.8)$$

This is a single scattering approximation for the cluttered field as we have neglected the term  $\mu U^{(1)}$  in this equation. Therefore  $U^{(1)}$  is given by

$$U^{(1)}(\mathbf{x}) = -\omega^2 \int_{\Omega} N_\omega^{(0)}(\mathbf{x}, \mathbf{y}) \mu(\mathbf{y}) U^{(0)}(\mathbf{y}) d\mathbf{y}.$$

- The second term of the right-hand side of (4.7) requires to model the term  $N_\omega$ . In the weak fluctuation regime, the error in this term is essentially determined by the phase mismatch between  $N_\omega(\mathbf{x}, \mathbf{z}_a)$  and  $\Lambda^{(0)}[N_\omega^{(0)}(\cdot, \mathbf{z}^S)](\mathbf{x})$  when  $\mathbf{z}^S$  is close to  $\mathbf{z}_a$  (which is the position of the peak). This phase mismatch comes from the random fluctuations of the travel time between  $\mathbf{x}$  and  $\mathbf{z}_a$  which is approximately equal to the integral of  $\mu/2$  along the ray from  $\mathbf{x}$  to  $\mathbf{z}_a$ :

$$\overline{N_\omega(\mathbf{x}, \mathbf{z}_a)} \Lambda^{(0)}[N_\omega^{(0)}(\cdot, \mathbf{z}^S)](\mathbf{x}) \simeq \overline{N_\omega^{(0)}(\mathbf{x}, \mathbf{z}_a)} \Lambda^{(0)}[N_\omega^{(0)}(\cdot, \mathbf{z}^S)](\mathbf{x}) e^{-i\omega T(\mathbf{x})},$$

with

$$T(\mathbf{x}) \simeq \frac{|\mathbf{x} - \mathbf{z}_a|}{2} \int_0^1 \mu\left(\mathbf{z}_a + \frac{\mathbf{x} - \mathbf{z}_a}{|\mathbf{x} - \mathbf{z}_a|} s\right) ds.$$

Therefore  $w^{(0)}$  can be expanded as

$$\begin{aligned} w^{(0)}(\mathbf{z}^S) &= \omega^2 \int_{\Omega} \mu(\mathbf{y}) \overline{U^{(0)}(\mathbf{y})} \left[ \int_{\partial\Omega} N_\omega^{(0)}(\mathbf{x}, \mathbf{z}^S) \overline{\Lambda^{(0)}[N_\omega^{(0)}(\cdot, \mathbf{y})](\mathbf{x})} d\sigma(\mathbf{x}) \right] d\mathbf{y} \\ &+ \delta^d \omega^2 (K^{-1} - 1) |B| \overline{U^{(0)}(\mathbf{z}_a)} \int_{\partial\Omega} \Lambda^{(0)}[N_\omega^{(0)}(\cdot, \mathbf{z}^S)](\mathbf{x}) \overline{N_\omega^{(0)}(\mathbf{x}, \mathbf{z}_a)} e^{-i\omega T(\mathbf{x})} d\sigma(\mathbf{x}). \end{aligned}$$

If the correlation radius of the random process  $\mu$  is small, then the last integral is self-averaging and therefore

$$\begin{aligned} w^{(0)}(\mathbf{z}^S) &= \omega^2 \int_{\Omega} \mu(\mathbf{y}) \overline{U^{(0)}(\mathbf{y})} \left[ \int_{\partial\Omega} N_\omega^{(0)}(\mathbf{x}, \mathbf{z}^S) \overline{\Lambda^{(0)}[N_\omega^{(0)}(\cdot, \mathbf{y})](\mathbf{x})} d\sigma(\mathbf{x}) \right] d\mathbf{y} \\ &+ \delta^d \omega^2 (K^{-1} - 1) |B| \overline{U^{(0)}(\mathbf{z}_a)} \int_{\partial\Omega} \Lambda^{(0)}[N_\omega^{(0)}(\cdot, \mathbf{z}^S)](\mathbf{x}) \overline{N_\omega^{(0)}(\mathbf{x}, \mathbf{z}_a)} e^{-\frac{\omega^2 \text{var}(T(\mathbf{x}))}{2}} d\sigma(\mathbf{x}). \end{aligned}$$

Let us introduce the kernel

$$Q(\mathbf{z}^S, \mathbf{z}_a) := \operatorname{Re} \left\{ U^{(0)}(\mathbf{z}^S) \overline{U^{(0)}(\mathbf{z}_a)} \int_{\partial\Omega} \Lambda^{(0)}[N_\omega^{(0)}(\cdot, \mathbf{z}^S)](\mathbf{x}) \overline{N_\omega^{(0)}(\mathbf{x}, \mathbf{z}_a)} d\sigma(\mathbf{x}) \right\},$$

and the function

$$Q_0(\mathbf{z}^S) = \frac{\lambda^{3-d}}{\pi 2^{5-d}} |U^{(0)}(\mathbf{z}^S)|^2 \quad \text{for } d = 2 \text{ or } 3. \quad (4.9)$$

As shown in Section 3, we have

$$Q(\mathbf{z}^S, \mathbf{z}_a) = \operatorname{Re} \left\{ U^{(0)}(\mathbf{z}^S) \overline{U^{(0)}(\mathbf{z}_a)} \int_{\partial\Omega} \Gamma_\omega(\mathbf{x} - \mathbf{z}^S) \overline{\Gamma_\omega(\mathbf{x} - \mathbf{z}_a)} d\sigma(\mathbf{x}) \right\}.$$

Moreover, the function  $\mathbf{z}^S \rightarrow Q(\mathbf{z}^S, \mathbf{z}_a)$  is maximal for  $\mathbf{z}^S = \mathbf{z}_a$ , its maximal value is  $Q_0(\mathbf{z}_a)$  and the width of the peak of  $\mathbf{z}^S \rightarrow Q(\mathbf{z}^S, \mathbf{z}_a)$  centered at  $\mathbf{z}^S = \mathbf{z}_a$  is of the order of half the wavelength  $\lambda$ . We can express the topological derivative imaging functional in terms of the kernel  $Q$ :

$$\begin{aligned} \mathcal{I}_{\text{TD}}[U^{(0)}](\mathbf{z}^S) &\simeq \omega^4 (K'^{-1} - 1) |B'| \int_{\Omega} \mu(\mathbf{y}) Q(\mathbf{z}^S, \mathbf{y}) d\mathbf{y} \\ &\quad + \delta^d \omega^4 (K'^{-1} - 1) (K^{-1} - 1) |B'| |B| Q(\mathbf{z}^S, \mathbf{z}_a) e^{-\frac{\omega^2 \operatorname{Var}(T)}{2}}, \end{aligned} \quad (4.10)$$

where we have assumed that  $\operatorname{Var}(T(\mathbf{x}))$  is constant for  $\mathbf{x} \in \partial\Omega$  in order to simplify the analysis.

The topological derivative has the form of a peak centered at the location  $\mathbf{z}_a$  of the anomaly (second term of the right-hand side of (4.10)) buried in a zero-mean Gaussian field or speckle pattern (first term of the right-hand side of (4.10)) that we can characterize statistically.

On the one hand clutter noise reduces the height of the main peak by the damping factor  $e^{-\omega^2 \operatorname{Var}(T)/2}$  and on the other hand it induces random fluctuations of the image in the form of a speckle field. The covariance function of the speckle field is

$$\begin{aligned} \operatorname{Cov}(\mathcal{I}_{\text{TD}}(\mathbf{z}^S), \mathcal{I}_{\text{TD}}(\mathbf{z}^{S'})) &= \omega^8 (K'^{-1} - 1)^2 |B'|^2 \\ &\quad \times \int_{\Omega} \int_{\Omega} Q(\mathbf{z}^S, \mathbf{y}) C_\mu(\mathbf{y}, \mathbf{y}') Q(\mathbf{z}^{S'}, \mathbf{y}') d\mathbf{y} d\mathbf{y}', \end{aligned}$$

where  $C_\mu$  is the covariance function of the process  $\mu$ :  $C_\mu(\mathbf{y}, \mathbf{y}') = \mathbb{E}[\mu(\mathbf{y})\mu(\mathbf{y}')]$ .

If we assume that the process  $\mu$  is supported and stationary in  $\Omega_\mu \subset \Omega$ , that the correlation radius  $l_\mu$  of  $\mu$  is smaller than the wavelength, and if we denote by  $\sigma_\mu$  the standard deviation of  $\mu$ , then we have

$$\operatorname{Var}(T) \simeq \frac{1}{8} \sigma_\mu^2 \operatorname{diam}(\Omega_\mu) l_\mu,$$

and

$$\operatorname{Cov}(\mathcal{I}_{\text{TD}}(\mathbf{z}^S), \mathcal{I}_{\text{TD}}(\mathbf{z}^{S'})) \simeq \omega^8 (K'^{-1} - 1)^2 |B'|^2 \sigma_\mu^2 l_\mu^d \int_{\Omega_\mu} Q(\mathbf{z}^S, \mathbf{y}) Q(\mathbf{z}^{S'}, \mathbf{y}) d\mathbf{y}.$$

Since the typical width of the kernel  $Q$  is about half-a-wavelength, we can see that the correlation radius of the speckle field is of the order of half the wavelength, that is to say, of the same order as the main peak centered at the anomaly location. Therefore, there is no way to distinguish the main peak from the hot spots of the speckle field based on their shapes. Only the height of the main peak can allow it to be visible out of the speckle field.

It is interesting to notice that the variance of the speckle field depends on the diameter of the heterogeneous region  $\Omega_\mu$ , because  $Q(\mathbf{z}^S, \mathbf{y})^2$  decays as  $1/|\mathbf{z}^S - \mathbf{y}|^{d-1}$  since  $|\mathbf{z}^S - \mathbf{y}| \gg \lambda$ , so that

$$\text{Var}(\mathcal{I}_{\text{TD}}(\mathbf{z}^S)) \simeq \omega^8 (K'^{-1} - 1)^2 |B'|^2 \sigma_\mu^2 l_\mu^d Q_0^2(\mathbf{z}_a) \lambda^{d-1} \text{diam}(\Omega_\mu).$$

Therefore, a large heterogeneous domain implies large fluctuations in the topological derivative, and the peak centered at the anomaly location  $\mathbf{z}_a$  can be buried in these fluctuations. More quantitatively, the Signal-to-Noise Ratio (SNR) defined by

$$\text{SNR} = \frac{\mathbb{E}[\mathcal{I}_{\text{TD}}(\mathbf{z}_a)]}{\text{Var}(\mathcal{I}_{\text{TD}}(\mathbf{z}_a))^{1/2}}$$

is equal to

$$\text{SNR} = \frac{(K^{-1} - 1) \delta^d |B|}{\sigma_\mu} \frac{\lambda^{1/2}}{\lambda^d} \frac{\lambda^{d/2}}{\text{diam}(\Omega_\mu)^{1/2}} \frac{\lambda^{d/2}}{l_\mu^{d/2}} e^{-\frac{\pi^2}{2} \sigma_\mu^2 \frac{l_\mu}{\lambda^2}}. \quad (4.11)$$

As shown by (4.11), the SNR is proportional to the contrast  $(K^{-1} - 1)$  and the volume of the anomaly,  $\delta^d |B|$  over the standard deviation the noise,  $\sigma_\mu$ . Moreover, it depends on the dimensionless parameters  $l_\mu/\lambda$ ,  $\text{diam}(\Omega_\mu)/\lambda$ , and  $\delta/\lambda$ .

## 5. Stability with Respect to Measurement Noise.

**5.1. The Topological Derivative in the Presence of Measurement Noise.** We consider the case in which the field  $u_{\text{meas}}(\mathbf{x})$  measured at the surface of the domain is corrupted by an additive noise that we denote by  $\nu_{\text{noise}}(\mathbf{x})$ ,  $\mathbf{x} \in \partial\Omega$ . Again, in order to simplify the presentation, we suppose that  $\rho = 1$ .

If we assume that the surface of the domain  $\Omega$  is covered with sensors half the wavelength apart from each other and that the additive noises have variance  $\sigma_1^2$  and are independent from one sensor to the other one, then we can model the additive noise process  $\nu_{\text{noise}}$  by a Gaussian white noise with covariance function

$$\mathbb{E}[\nu_{\text{noise}}(\mathbf{x}) \overline{\nu_{\text{noise}}(\mathbf{x}')}] = \sigma_{\text{noise}}^2 \delta(\mathbf{x} - \mathbf{x}'), \quad \sigma_{\text{noise}}^2 = \sigma_1^2 \lambda^{d-1} 2^{1-d}.$$

The topological derivative imaging functional is

$$\mathcal{I}_{\text{TD}}[U^{(0)}](\mathbf{z}^S) = \omega^2 (K'^{-1} - 1) |B'| \text{Re}\{U^{(0)}(\mathbf{z}^S) (w^{(0)}(\mathbf{z}^S) + w_{\text{noise}}(\mathbf{z}^S))\},$$

where

$$w_{\text{noise}}(\mathbf{z}^S) = -\mathcal{S}_\Omega^{\omega, (0)} \overline{\left(-\frac{1}{2}\mathcal{I} + \mathcal{K}_\Omega^{\omega, (0)}\right)[\nu_{\text{noise}}](\mathbf{z}^S)}, \quad (5.1)$$

and

$$w^{(0)}(\mathbf{z}^S) = \mathcal{S}_\Omega^{\omega, (0)} \overline{\left(-\frac{1}{2}\mathcal{I} + \mathcal{K}_\Omega^{\omega, (0)}\right)[U^{(0)} - (u_{\text{meas}} - \nu_{\text{noise}})](\mathbf{z}^S)}. \quad (5.2)$$

**5.2. Stability and Resolution Analysis.** We find from (5.1) and (5.2) that

$$\begin{aligned} \mathcal{I}_{\text{TD}}[U^{(0)}](\mathbf{z}^S) &= \delta^d \omega^4 (K'^{-1} - 1) (K^{-1} - 1) |B'| \overline{|B| Q(\mathbf{z}^S, \mathbf{z}_a) - \omega^2 (K'^{-1} - 1) |B'|} \\ &\times \text{Re}\left\{ \int_{\partial\Omega} U^{(0)}(\mathbf{z}^S) \Gamma_\omega(\mathbf{z}^S - \mathbf{y}) \overline{\left(-\frac{1}{2}\mathcal{I} + \mathcal{K}_\Omega^{\omega, (0)}\right)[\nu_{\text{noise}}](\mathbf{y})} d\sigma(\mathbf{y}) \right\}. \end{aligned} \quad (5.3)$$

Therefore, the imaging functional  $\mathcal{I}_{\text{TD}}$  has the form of a peak centered at the location  $\mathbf{z}_a$  of the anomaly. Moreover, (5.3) shows that the peak is buried in a

speckle field, as in the case of clutter noise. However, on contrary to the clutter noise, the value of the main peak itself is not reduced by the additive noise, which means that the imaging functional is much more robust with respect to additive measurement noise than with respect to clutter noise. Let us compute the covariance function of the speckle field. We first introduce the auxiliary field defined on  $\partial\Omega$ :

$$\nu_{\text{noise},1}(\mathbf{y}) = \left(-\frac{1}{2}\mathcal{I} + \mathcal{K}_\Omega^{\omega,(0)}\right)[\nu_{\text{noise}}](\mathbf{y}).$$

It is a zero-mean with Gaussian statistics and covariance

$$\begin{aligned} \mathbb{E}[\nu_{\text{noise},1}(\mathbf{y})\overline{\nu_{\text{noise},1}(\mathbf{y}')} ] &= \frac{\sigma_{\text{noise}}^2}{4}\delta(\mathbf{y} - \mathbf{y}') - \frac{\sigma_{\text{noise}}^2}{2}\left(\frac{\partial\Gamma_\omega(\mathbf{y}' - \mathbf{y})}{\partial\nu(\mathbf{y})} + \frac{\partial\Gamma_\omega(\mathbf{y}' - \mathbf{y})}{\partial\nu(\mathbf{y}')}\right) \\ &\quad + \sigma_{\text{noise}}^2 \int_{\partial\Omega} \frac{\partial\Gamma_\omega(\mathbf{y} - \mathbf{x})}{\partial\nu(\mathbf{x})} \overline{\frac{\partial\Gamma_\omega(\mathbf{y}' - \mathbf{x})}{\partial\nu(\mathbf{x})}} d\sigma(\mathbf{x}). \end{aligned}$$

We next introduce the auxiliary field defined on  $\Omega$ :

$$\nu_{\text{noise},2}(\mathbf{z}) = \int_{\partial\Omega} \Gamma_\omega(\mathbf{z} - \mathbf{y})\overline{\nu_{\text{noise},1}(\mathbf{y})} d\sigma(\mathbf{y}).$$

It is a zero-mean with Gaussian statistics with covariance:

$$\mathbb{E}[\nu_{\text{noise},2}(\mathbf{z})\overline{\nu_{\text{noise},2}(\mathbf{z}')} ] = \int_{\partial\Omega} \int_{\partial\Omega} \Gamma_\omega(\mathbf{z} - \mathbf{y})\overline{\Gamma_\omega(\mathbf{z}' - \mathbf{y}')} \mathbb{E}[\nu_{\text{noise},1}(\mathbf{z})\overline{\nu_{\text{noise},1}(\mathbf{z}')} ] d\sigma(\mathbf{y}) d\sigma(\mathbf{y}').$$

Using Helmholtz-Kirchhoff theorem the covariance of  $\nu_{\text{noise},2}(\mathbf{z})$  can be expressed as

$$\begin{aligned} \mathbb{E}[\nu_{\text{noise},2}(\mathbf{z})\overline{\nu_{\text{noise},2}(\mathbf{z}')} ] &= \frac{\sigma_{\text{noise}}^2}{4\omega} \text{Im}\{\Gamma_\omega(\mathbf{z} - \mathbf{z}')\} \\ &\quad - \frac{\sigma_{\text{noise}}^2}{2\omega} \int_{\partial\Omega} \Gamma_\omega(\mathbf{z} - \mathbf{y}) \frac{\partial\text{Im}\{\Gamma_\omega(\mathbf{z}' - \mathbf{y})\}}{\partial\nu(\mathbf{y})} d\sigma(\mathbf{y}) \\ &\quad - \frac{\sigma_{\text{noise}}^2}{2\omega} \int_{\partial\Omega} \overline{\Gamma_\omega(\mathbf{z}' - \mathbf{y})} \frac{\partial\text{Im}\{\Gamma_\omega(\mathbf{z} - \mathbf{y})\}}{\partial\nu(\mathbf{y})} d\sigma(\mathbf{y}) \\ &\quad + \frac{\sigma_{\text{noise}}^2}{\omega^2} \int_{\partial\Omega} \frac{\partial\text{Im}\{\Gamma_\omega(\mathbf{z} - \mathbf{y})\}}{\partial\nu(\mathbf{y})} \overline{\frac{\partial\text{Im}\{\Gamma_\omega(\mathbf{z}' - \mathbf{y})\}}{\partial\nu(\mathbf{y})}} d\sigma(\mathbf{y}). \end{aligned}$$

When  $\mathbf{z}$  and  $\mathbf{z}'$  are far from the boundary, using  $\frac{\partial\Gamma_\omega(\mathbf{z} - \mathbf{y})}{\partial\nu(\mathbf{y})} \simeq i\omega\Gamma_\omega(\mathbf{z} - \mathbf{y})$  and Helmholtz-Kirchhoff theorem, we get

$$\mathbb{E}[\nu_{\text{noise},2}(\mathbf{z})\overline{\nu_{\text{noise},2}(\mathbf{z}')} ] = \frac{\sigma_{\text{noise}}^2}{4\omega} \text{Im}\{\Gamma(\mathbf{z} - \mathbf{z}')\},$$

and therefore

$$\text{Cov}(\mathcal{I}_{\text{TD}}(\mathbf{z}^S), \mathcal{I}_{\text{TD}}(\mathbf{z}^{S'})) = \frac{1}{8}\omega^4(K'^{-1} - 1)^2|B'|^2\sigma_{\text{noise}}^2 Q(\mathbf{z}^S, \mathbf{z}^{S'}),$$

for the search points  $\mathbf{z}^S, \mathbf{z}^{S'} \in \Omega$ . This shows that the typical shape of a hot spot of the speckle field is exactly the form of the main peak. Moreover, the variance of the speckle field is

$$\text{Var}(\mathcal{I}_{\text{TD}}(\mathbf{z}^S)) = \frac{1}{8}\omega^4(K'^{-1} - 1)^2|B'|^2\sigma_{\text{noise}}^2 Q_0(\mathbf{z}^S),$$

with  $Q_0$  given by (4.9), which shows that the SNR is equal to

$$\text{SNR} = \frac{2\sqrt{2}\omega^2 Q_0(\mathbf{z}_a)^{1/2} (K^{-1} - 1)\delta^d |B|}{\sigma_{\text{noise}}} = 2^{d-1} \pi^{3/2} \frac{|U^{(0)}(\mathbf{z}_a)| (K^{-1} - 1) \delta^d |B|}{\sigma_1 \lambda^d}. \quad (5.4)$$

From (5.4), the SNR is proportional to the contrast  $(K^{-1} - 1)$  and the volume of the anomaly,  $\delta^d |B|$ , over the standard deviation of the noise,  $\sigma_{\text{noise}}$ .

**6. Other Imaging Algorithms.** Consider  $P$  well-separated anomalies  $D_p = \mathbf{z}_p + \delta B_p$ ,  $p = 1, \dots, P$ . The volumetric mass density and bulk modulus of  $D_p$  are denoted by  $\rho_p$  and  $K_p$ , respectively. Suppose that all the domains  $B_p$  are disks.

**6.1. MUSIC-type Algorithm.** Let  $(\boldsymbol{\theta}_1, \dots, \boldsymbol{\theta}_n)$  be  $n$  unit vectors in  $\mathbb{R}^d$ . For  $\boldsymbol{\theta} \in \{\boldsymbol{\theta}_1, \dots, \boldsymbol{\theta}_n\}$ , we assume that we are in possession of the boundary data  $u$  when the domain  $\Omega$  is illuminated with the plane wave  $U(\mathbf{x}) = e^{i\omega\boldsymbol{\theta}^T\mathbf{x}}$ . Therefore, taking the harmonic function  $w(\mathbf{x}) = e^{-i\omega\boldsymbol{\theta}'^T\mathbf{x}}$  for  $\boldsymbol{\theta}' \in \{\boldsymbol{\theta}_1, \dots, \boldsymbol{\theta}_n\}$  and using (2.3) shows that the weighted boundary measurement is approximately equal to

$$I_w[U, \omega] \simeq - \sum_{p=1}^P |D_p| \omega^2 \left( 2 \frac{\rho_p^{-1} - 1}{\rho_p^{-1} + 1} \boldsymbol{\theta}^T \boldsymbol{\theta}' + K_p^{-1} - 1 \right) e^{i\omega(\boldsymbol{\theta} - \boldsymbol{\theta}')^T \mathbf{z}_p}.$$

Define the response matrix  $\mathbf{A} = (A_{ll'})_{l, l'=1}^n \in \mathbb{C}^{n \times n}$  by

$$A_{ll'} := I_{w_{l'}}[U_l, \omega]. \quad (6.1)$$

It is approximately given by

$$A_{ll'} \simeq - \sum_{p=1}^P |D_p| \omega^2 \left( 2 \frac{\rho_p^{-1} - 1}{\rho_p^{-1} + 1} \boldsymbol{\theta}_l^T \boldsymbol{\theta}_{l'} + K_p^{-1} - 1 \right) e^{i\omega(\boldsymbol{\theta}_l - \boldsymbol{\theta}_{l'})^T \mathbf{z}_p},$$

for  $l, l' = 1, \dots, n$ . Introduce the  $n$ -dimensional vector fields  $\mathbf{g}^{(j)}$ , defined for  $j = 1, \dots, d+1$ , by

$$\mathbf{g}^{(j)}(\mathbf{x}) = (\mathbf{e}_j^T \boldsymbol{\theta}_1 e^{i\omega\boldsymbol{\theta}_1^T \mathbf{x}}, \dots, \mathbf{e}_j^T \boldsymbol{\theta}_n e^{i\omega\boldsymbol{\theta}_n^T \mathbf{x}})^T, \quad j = 1, \dots, d, \quad (6.2)$$

and

$$\mathbf{g}^{(d+1)}(\mathbf{x}) = (e^{i\omega\boldsymbol{\theta}_1^T \mathbf{x}}, \dots, e^{i\omega\boldsymbol{\theta}_n^T \mathbf{x}})^T, \quad (6.3)$$

where  $(\mathbf{e}_1, \dots, \mathbf{e}_d)$  is an orthonormal basis of  $\mathbb{R}^d$ . Let  $\mathbf{P}_{\text{noise}} = \mathbf{I} - \mathbf{P}$ , where  $\mathbf{P}$  is the orthogonal projection onto the range of  $\mathbf{A}$ . The MUSIC-type imaging functional is defined by

$$\mathcal{I}_{\text{MU}}(\mathbf{z}^S) := \left( \sum_{j=1}^{d+1} \|\mathbf{P}_{\text{noise}} \mathbf{g}^{(j)}(\mathbf{z}^S)\|^2 \right)^{-1/2}. \quad (6.4)$$

This functional has large peaks only at the locations of the anomalies; see, *e.g.*, [1].

**6.2. Backpropagation-type Algorithms.** Let  $(\boldsymbol{\theta}_1, \dots, \boldsymbol{\theta}_n)$  be  $n$  unit vectors in  $\mathbb{R}^d$ . A backpropagation-type imaging functional at a single frequency  $\omega$  is given by

$$\mathcal{I}_{\text{BP}}(\mathbf{z}^S) := \frac{1}{n} \sum_{l=1}^n e^{-2i\omega\boldsymbol{\theta}_l^T \mathbf{z}^S} I_{w_l}[U_l, \omega], \quad (6.5)$$

where  $U_l(\mathbf{x}) = w_l(\mathbf{x}) = e^{i\omega\boldsymbol{\theta}_l^T \mathbf{x}}$ ,  $l = 1, \dots, n$ . Suppose that  $(\boldsymbol{\theta}_1, \dots, \boldsymbol{\theta}_n)$  are equidistant points on the unit sphere  $S^{d-1}$ . For sufficiently large  $n$ , we have (3.8) and it follows that

$$\mathcal{I}_{\text{BP}}(\mathbf{z}^S) \simeq \sum_{p=1}^P |D_p| \omega^2 \left( 2 \frac{\rho_p^{-1} - 1}{\rho_p^{-1} + 1} - (K_p^{-1} - 1) \right) \times \begin{cases} \text{sinc}(2\omega|\mathbf{z}^S - \mathbf{z}_p|) & \text{for } d = 3, \\ J_0(2\omega|\mathbf{z}^S - \mathbf{z}_p|) & \text{for } d = 2. \end{cases}$$

These formulae show that the resolution of the imaging functional is the standard diffraction limit. Note that the above backpropagation-type algorithm is a simplified

version of the algorithm studied in [2, 3]. In fact, instead of using only the diagonal terms of the response matrix  $\mathbf{A}$ , defined by (6.1), we can use the whole matrix to define the Kirchhoff migration functional:

$$\mathcal{I}_{\text{KM}}(\mathbf{z}^S) = \sum_{j=1}^{d+1} \sum_l \left( \overline{\mathbf{g}^{(j)}(\mathbf{z}^S)}^T \mathbf{u}_l \right) \left( \overline{\mathbf{g}^{(j)}(\mathbf{z}^S)}^T \mathbf{v}_l \right), \quad (6.6)$$

where  $\mathbf{u}_l$  and  $\mathbf{v}_l$  are respectively the left and right singular vectors of  $\mathbf{A}$  and  $\mathbf{g}^{(j)}$  are defined by (6.2) and (6.3).

**7. Numerical Illustrations.** In this section we present results of numerical experiments that give qualitative illustrations of some of the main findings in this paper. We consider the two-dimensional case ( $d = 2$ ). The domain  $\Omega$  is the unit disk. We simulate the measurements using a finite-element method to solve the Helmholtz equation. We use a piecewise linear representation of the solution  $u$  and piecewise constant representations of the parameter distributions  $\mathbf{1}_{\Omega \setminus \overline{D}}(\mathbf{x}) + \rho^{-1} \mathbf{1}_D(\mathbf{x})$  and  $\mathbf{1}_{\Omega \setminus \overline{D}}(\mathbf{x}) + K^{-1} \mathbf{1}_D(\mathbf{x})$ . We consider a small anomaly  $D = \mathbf{z}_a + \delta B$  with  $\mathbf{z}_a = (-0.3, 0.5)$ ,  $\delta = 0.05$ , and  $B$  being the unit disk. We fix the working frequency  $\omega$  to be equal to 6, which corresponds to a wavelength  $\lambda \simeq 1$ . We assume that the measurements corresponding to the plane wave illuminations,  $U_l(\mathbf{x}) = e^{i\omega \boldsymbol{\theta}_l^T \mathbf{x}}$ , at the equi-distributed directions  $\boldsymbol{\theta}_l$ , for  $l = 1, \dots, n = 50$ .

**7.1. Bulk Modulus Contrast Only.** Here, the parameters of the anomaly are  $\rho = 1$  and  $K = 1/2$ .

**7.1.1. Resolution in the Absence of Noise.** Within the above setting, we first present results of the described algorithms in the absence of noise. In Figure 7.1, plots of  $\mathcal{I}_{\text{TD}}(\mathbf{z}^S)$ , defined by (3.11), with respectively  $n = 50$  and  $n = 2$  illustrate the efficiency of the proposed topological derivative based imaging procedure. The imaging functional  $\mathcal{I}_{\text{TD}}(\mathbf{z}^S)$  reaches its maximum at the location  $\mathbf{z}_a$  of the anomaly and behaves, accordingly to (3.9), like  $J_0(\omega|\mathbf{z}^S - \mathbf{z}_a|)^2$  if the number  $n$  of incident waves is large while for small  $n$ , it behaves, as expected, like  $J_0(\omega|\mathbf{z}^S - \mathbf{z}_a|)$ .

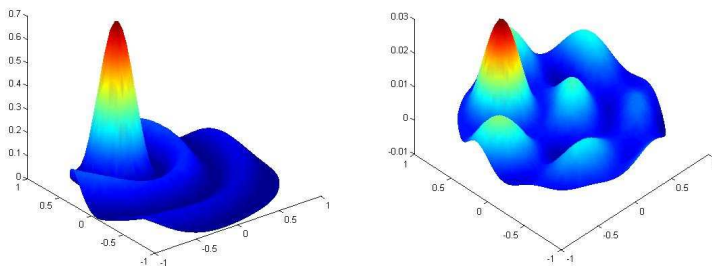


FIG. 7.1. Plots of  $\mathcal{I}_{\text{TD}}(\mathbf{z}^S)$  defined by (3.11) with  $n = 50$  (left) and  $n = 2$  (right).

In Figures 7.2 and 7.3, we compare the performance of the topological based imaging functionals with and without postprocessing the data by applying the integral operator  $(-\frac{1}{2}\mathcal{I} + \mathcal{K}_\Omega^\omega)$ . It is clear that the data postprocessing step is essential, specially if the number  $n$  of incident waves is small. In Figure 7.4, we show that this postprocessing is even more essential in the case of multiple anomalies.

In Figure 7.5, we present two MUSIC-type reconstructions. Given the structure of the response matrix  $\mathbf{A}$  with  $\rho = 1$  (contrast only on the  $K$  distribution), it is

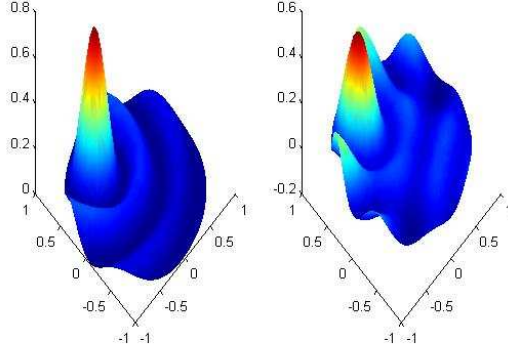


FIG. 7.2. Comparison for  $n = 50$  between topological derivative based images with (left) and without (right) postprocessing the data.

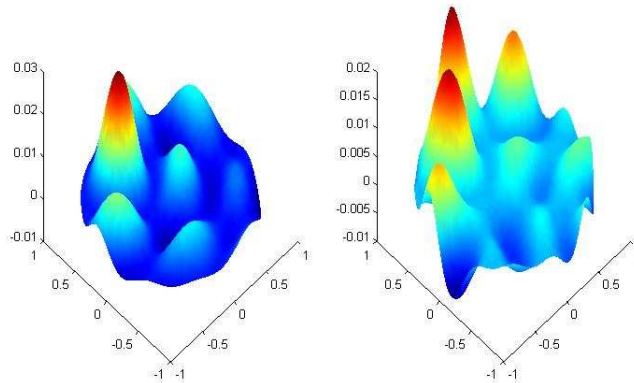


FIG. 7.3. Comparison for  $n = 2$  between topological derivative based images with (left) and without (right) postprocessing the data.

known that its SVD yields only one significant singular value. See, *e.g.*, [4, 1]. Thus, the illumination vectors  $\mathbf{g}^{(1)}$  and  $\mathbf{g}^{(2)}$  do not belong to the signal subspace of  $\mathbf{A}$ . Using these vectors in the projection step generates a blurred MUSIC image (figure on the left). To get a sharp peak, we should project only the illumination vector  $\mathbf{g}^{(3)}$  (figure on the right), which assumes a priori knowledge of the physical nature of the contrast.

As shown in Figure 7.6, the backpropagation image of the anomaly has the expected behavior of the Bessel function and reaches its maximum at the location of the anomaly.

### 7.1.2. Stability with Respect to Measurement and Medium Noises.

We now consider imaging from noisy data. We first add electronic (measurement) noise  $\nu_{\text{noise}}$  to the previous measurements  $u_{i,\text{meas}}$ ,  $i = 1, \dots, n$ . Here,  $\nu_{\text{noise}}$  is a white Gaussian noise with standard deviation  $\sigma\%$  of the  $L^2$  norm of  $u_{\text{meas}}$  and  $\sigma$

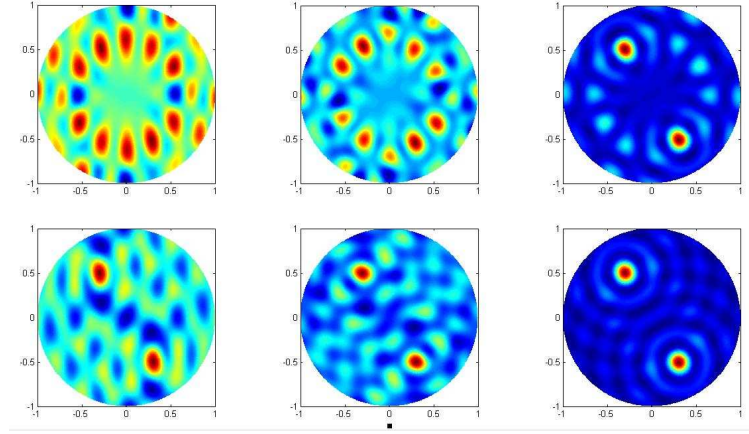


FIG. 7.4. Comparison between topological derivative based images of multiple anomalies with (second line) and without (first line) postprocessing the data. The first column corresponds to  $n = 1$ , the second to  $n = 2$ , and the third to  $n = 50$ .

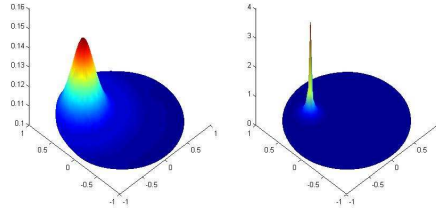


FIG. 7.5. Left: MUSIC image using the projection of  $\mathbf{g}^{(1)}, \mathbf{g}^{(2)}$ , and  $\mathbf{g}^{(3)}$  on the signal subspace of  $\mathbf{A}$ . Right: MUSIC image using the projection of  $\mathbf{g}^{(3)}$  on the signal subspace of  $\mathbf{A}$ .

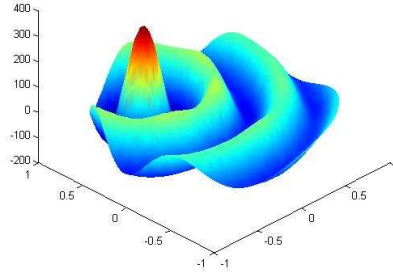


FIG. 7.6. Plot of  $\mathcal{I}_{\text{BP}}(\mathbf{z}^S)$  defined by (6.5) with  $n = 50$ .

ranges from 0 to 30. We compute  $N_r = 250$  realizations of such noise and apply different imaging algorithms. Figure 7.7 presents the results of computational experiments. It clearly shows that the topological derivative based functional performs as good as Kirchhoff migration and much better than MUSIC and backpropagation, specially at high levels of electronic noise. Figure 7.8 shows the dramatic effect of the postprocessing step in the topological derivative based imaging when the number of plane wave illuminations  $n$  is small.

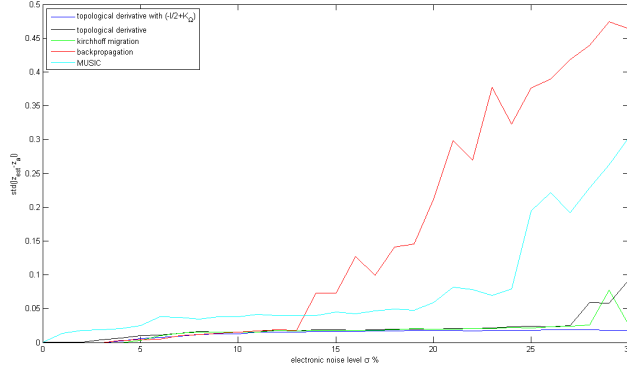


FIG. 7.7. Standard deviations of localization error with respect to electronic noise level for  $\mathcal{I}_{\text{MU}}$ ,  $\mathcal{I}_{\text{BP}}$ ,  $\mathcal{I}_{\text{KM}}$ , and  $\mathcal{I}_{\text{TD}}$  with  $n = 50$ .

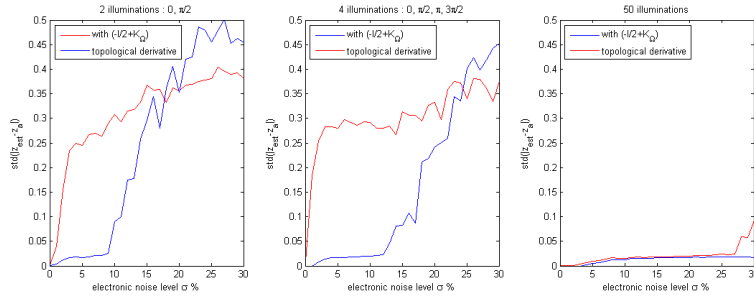


FIG. 7.8. Effect of the data postprocessing on the standard deviation of localization error with respect to electronic noise level.

We now suppose that the medium bulk modulus is randomly heterogeneous around a constant background:  $K^{-1}(\mathbf{x}) = 1 + (K^{-1} - 1)\mathbf{1}_D(\mathbf{x}) + \mu(\mathbf{x})$ . To simulate  $\mu$ , we compute a white Gaussian noise in the medium and then apply a low-pass Gaussian filter. The parameters of this filter can be linked to the correlation length  $l_\mu$  of  $\mu$ .

Comparisons between the standard deviations of the localization error with respect to clutter noise for the discussed imaging algorithms are given in Figures 7.9 and 7.10. Again, the topological derivative based imaging functional is the most robust functional.

**7.2. Density Contrast Only.** Here, the parameters of the anomaly are  $\rho = 1/2$  and  $K = 1$ .

**7.2.1. Resolution in the Absence of Noise.** As shown in Figure 7.11, the topological derivative based imaging functional  $\mathcal{I}_{\text{TD}}(\mathbf{z}^S)$  reaches its maximum at the location of the anomaly.

In Figures 7.12 and 7.13, we compare the performance of the topological based imaging functionals with and without the postprocessing step. In Figure 7.14, we show that this postprocessing is even more critical in the case of multiple anomalies.

Figure 7.15 shows MUSIC images. As expected from the structure of the response matrix with  $K = 1$  ( $\rho$  contrast only), its SVD yields two significant singular values [10, 4, 1]. Thus, the illumination vector  $\mathbf{g}^{(3)}$  does not belong to the signal subspace of the response matrix  $\mathbf{A}$ . As before, using this vector in the projection step generates a blurred MUSIC peak (figure on the left). To get a sharp peak, we

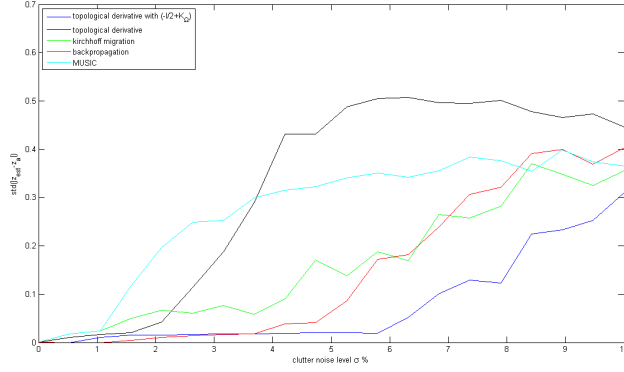


FIG. 7.9. Standard deviations of localization error with respect to clutter noise for  $\mathcal{I}_{MU}$ ,  $\mathcal{I}_{BP}$ ,  $\mathcal{I}_{KM}$ , and  $\mathcal{I}_{TD}$  with  $n = 50$ .

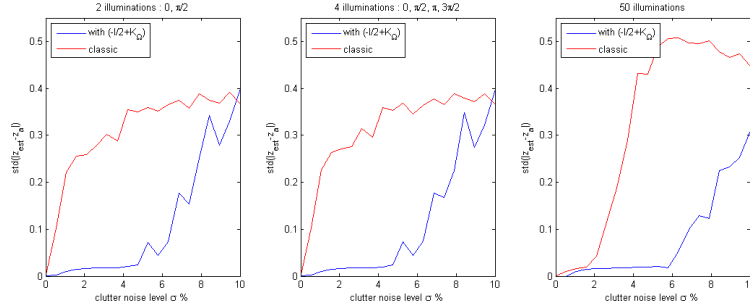


FIG. 7.10. Effect of the data postprocessing on the standard deviation of localization error with respect to clutter noise.

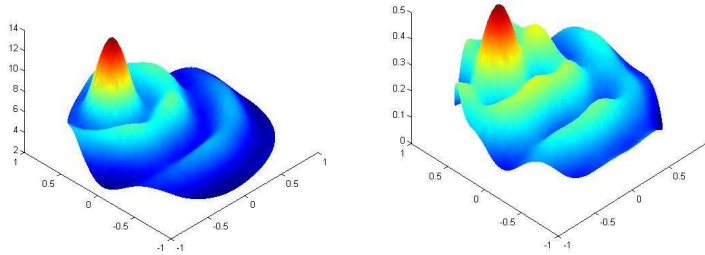


FIG. 7.11. Plots of  $\mathcal{I}_{TD}(z^S)$  with (left)  $n = 50$  and (right)  $n = 2$ .

should only project the illumination vectors  $\mathbf{g}^{(1)}$  and  $\mathbf{g}^{(2)}$  (figure on the right).

As shown in Figure 7.16, the backpropagation image has the expected behavior and reaches its maximum at the location of the anomaly. In the case of multiple anomalies, the oscillatory pattern of the backpropagation imaging functional can be troublesome.

### 7.2.2. Stability with Respect to Measurement and Medium Noises.

We carry out the same analysis as in the case of only a bulk modulus contrast. Figure 7.17 gives the standard deviation of the localization error as function of the

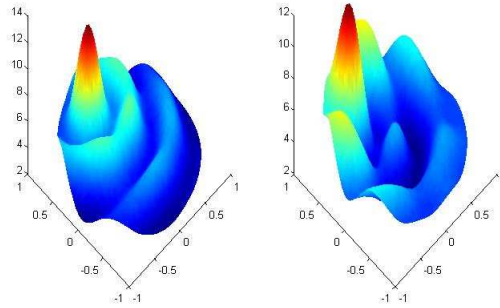


FIG. 7.12. Comparison for  $n = 50$  between topological derivative based images with (left) and without (right) postprocessing the data.

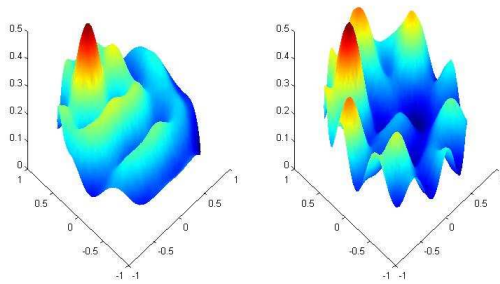


FIG. 7.13. Comparison for  $n = 2$  between topological derivative based images with (left) and without (right) postprocessing the data.

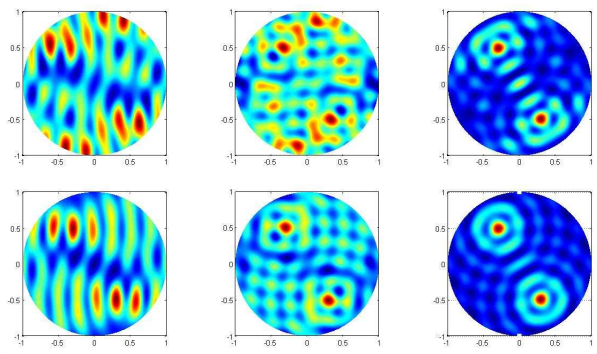


FIG. 7.14. Comparison between topological derivative based images of multiple anomalies with (second line) and without (first line) postprocessing the data. The first column corresponds to  $n = 1$ , the second to  $n = 2$ , and the third to  $n = 50$ .

noise level  $\sigma$  for each algorithm.

Again, the topological derivative algorithm with postprocessing seems to be the most robust. However, the effect of the data postprocessing step seems less

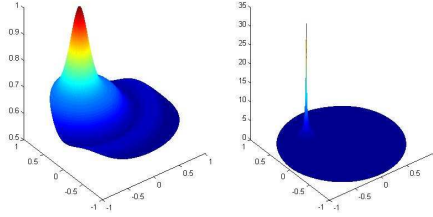


FIG. 7.15. Left: MUSIC image using projection of  $\mathbf{g}^{(1)}, \mathbf{g}^{(2)}, \mathbf{g}^{(3)}$  on the signal subspace of  $\mathbf{A}$ . Right: image using projection of  $\mathbf{g}^{(1)}$  and  $\mathbf{g}^{(2)}$  on the signal subspace of  $\mathbf{A}$ .

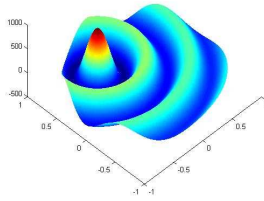


FIG. 7.16. Backpropagation image.

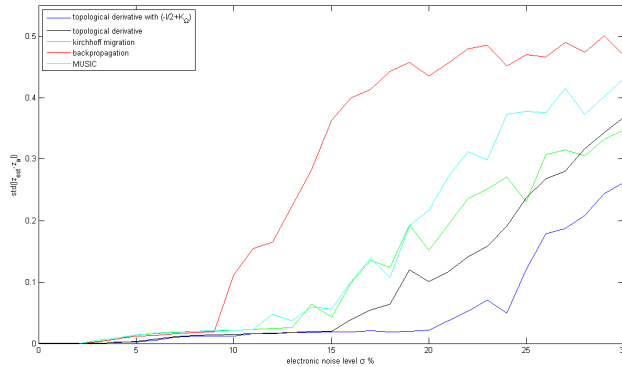


FIG. 7.17. Standard deviations of localization error with respect to electronic noise level for  $\mathcal{I}_{\text{MU}}, \mathcal{I}_{\text{BP}}, \mathcal{I}_{\text{KM}},$  and  $\mathcal{I}_{\text{TD}}$  with  $n = 50$ .

dramatic here than in the case of bulk modulus contrast.

Finally, we suppose that the medium density is randomly heterogeneous around a constant background:  $\rho^{-1}(\mathbf{x}) = 1 + (\rho^{-1} - 1)\mathbf{1}_D(\mathbf{x}) + \mu(\mathbf{x})$ , with  $\mu$  a random process of mean zero and tunable standard deviation  $\sigma$ . As before, we compute  $N_r = 250$  realizations of such clutter and the corresponding measurements. We then apply the localization algorithms. Stability results are given in Figure 7.19. They clearly indicate the robustness of the topological derivative based imaging functional.

**8. Conclusion.** In this paper we have explained why the concept of topological derivative works for imaging small acoustic anomalies and carried out a stability and resolution analysis in the presence of medium and measurement noises. We have shown that in order to design an efficient topological derivative based imaging functional, we have first to postprocess the data. We have proved that the

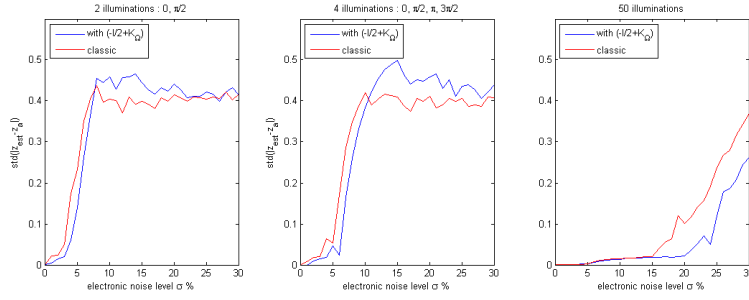


FIG. 7.18. Standard deviations of localization error with respect to electronic noise level for the topological derivative based functionals with and without postprocessing the data.

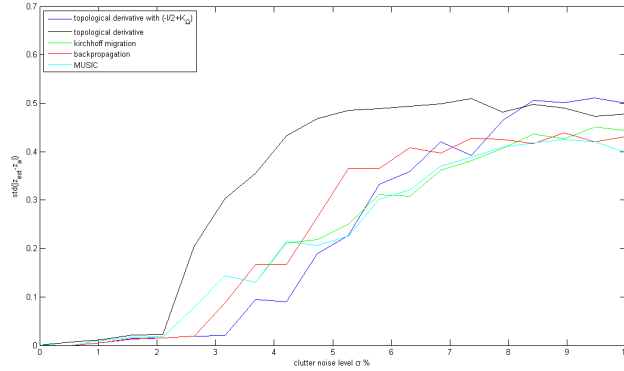


FIG. 7.19. Standard deviations of the localization error with respect to clutter noise for  $\mathcal{I}_{\text{MU}}$ ,  $\mathcal{I}_{\text{BP}}$ ,  $\mathcal{I}_{\text{KM}}$ , and  $\mathcal{I}_{\text{TD}}$  with  $n = 50$ .

functional behaves like the square of the imaginary part of the Green function and then attains its maximum at the location of the anomaly with a resolution limit of the order of half-a-wavelength. We have also shown that the topological derivative based imaging functional, compared to other more classical imaging functionals, is more robust in both cases of measurement and medium noise. Another advantage of the proposed functional is that it works with a very small number of plane wave illuminations. However, its complexity is roughly speaking  $O(nm^3)$  while the complexities of MUSIC and backpropagation are respectively  $O(n^3 + n^2m)$  and  $O(nm)$ , where  $n$  is the number of plane wave illuminations and  $m$  is the number of space discretization points in the domain  $\Omega$ . Note that in general  $n \ll m$ .

Our results in this paper apply to the electrical impedance tomography problem. In fact, let  $\Gamma$  be the fundamental solution of the Laplacian in  $\mathbb{R}^d$  and denote by  $\mathcal{K}_\Omega$  the integral operator given by

$$\mathcal{K}_\Omega[\varphi](\mathbf{x}) = \int_{\partial\Omega} \frac{\partial\Gamma(\mathbf{x} - \mathbf{y})}{\partial\nu(\mathbf{y})} \varphi(\mathbf{y}) d\sigma(\mathbf{y}), \quad \mathbf{x} \in \partial\Omega.$$

Let  $\mathcal{I}_{\text{TD}}$  be the topological derivative of the misfit

$$\mathcal{E}[U](\mathbf{z}^S) = \frac{1}{2} \int_{\partial\Omega} |(-\frac{1}{2}\mathcal{I} + \mathcal{K}_\Omega)[u_{\mathbf{z}^S} - u_{\text{meas}}](\mathbf{x})|^2 d\sigma(\mathbf{x}),$$

where  $u_{\mathbf{z}^S}$  and  $u_{\text{meas}}$  are respectively the computed and the measured voltage potential. In exactly the same manner as in this paper, we can prove that, for  $d = 2$ ,

$$\mathcal{I}_{\text{TD}}(\mathbf{z}^S) \sim \int_{\partial\Omega} \nabla\Gamma(\mathbf{x} - \mathbf{z}^S) \nabla\Gamma(\mathbf{x} - \mathbf{z}_a) d\sigma(\mathbf{x}) \sim \int_{\partial\Omega} \frac{1}{|\mathbf{x}|^2} \frac{(\mathbf{x} - \mathbf{z}^S)^T (\mathbf{x} - \mathbf{z}_a)}{|\mathbf{x} - \mathbf{z}^S| |\mathbf{x} - \mathbf{z}_a|} d\sigma(\mathbf{x})$$

provided that  $\text{dist}(\mathbf{z}^S, \partial\Omega), \text{dist}(\mathbf{z}_a, \partial\Omega) \gg 1$ . A similar result holds in three dimensions. Therefore,  $\mathcal{I}_{\text{TD}}(\mathbf{z}^S)$  yields an image similar to the one proposed in [18].

Our results extend to elastic and electromagnetic waves as well as to the transient regime [19]. They can also be generalized to imaging functionals based on high-order topological derivatives [8, 22, 17], which are based on high-order asymptotic expansions for the boundary pressure perturbations derived in [5].

#### REFERENCES

- [1] H. Ammari, *An Introduction to Mathematics of Emerging Biomedical Imaging*, Mathematics & Applications, Vol. 62, Springer-Verlag, Berlin, 2008.
- [2] H. Ammari, J. Garnier, H. Kang, W.-K. Park, and K. Sølna, Imaging schemes for perfectly conducting cracks, *SIAM J. Appl. Math.*, to appear.
- [3] H. Ammari, J. Garnier, and K. Sølna, A statistical approach to target detection and localization in the presence of noise, *Waves in Random and Complex Media*, to appear.
- [4] H. Ammari, E. Iakovleva, and D. Lesselier, A MUSIC algorithm for locating small inclusions buried in a half-space from the scattering amplitude at a fixed frequency, *Multiscale Model. Simul.*, 3 (2005), 597–628.
- [5] H. Ammari and H. Kang, *Reconstruction of Small Inhomogeneities from Boundary Measurements*, Lecture Notes in Mathematics, Vol. 1846, Springer-Verlag, Berlin, 2004.
- [6] H. Ammari and H. Kang, *Polarization and Moment Tensors: with Applications to Inverse Problems and Effective Medium Theory*, Applied Mathematical Sciences, Vol. 162, Springer-Verlag, New York, 2007.
- [7] H. Ammari, H. Kang, and H. Lee, *Layer Potential Techniques in Spectral Analysis*, Mathematical Surveys and Monographs, Vol. 153, American Mathematical Society, Providence RI, 2009.
- [8] M. Bonnet, Higher-order topological sensitivity for 2-D potential problems. Application to fast identification of inclusions, *Inter. J. Solids Struct.*, 46 (2009), 2275–2292.
- [9] M. Bonnet and B. B. Guzina, Sounding of finite solid bodies by way of topological derivative, *Int. J. Numer. Meth. Eng.*, 61 (2004), 2344–2373.
- [10] M. Brühl, M. Hanke, and M. S. Vogelius, A direct impedance tomography algorithm for locating small inhomogeneities, *Numer. Math.*, 93 (2003), 635–654.
- [11] J. Céa, S. Garreau, P. Guillaume, and M. Masmoudi, The shape and topological optimization connection, *Computer Methods in Applied Mechanics and Engineering*, 188 (2001), 703–726.
- [12] N. Dominguez, V. Gibiat and Y. Esquerrea, Time domain topological gradient and time reversal analogy: an inverse method for ultrasonic target detection, *Wave Motion*, 42 (2005), 31–52.
- [13] N. Dominguez and V. Gibiat, Non-destructive imaging using the time domain topological energy method, *Ultrasonics*, 50 (2010), 172–179.
- [14] H. A. Eschenauer, V. V. Koblelev, and A. Schumacher, Bubble method for topology and shape optimization of structures, *Struct. Optimization* 8 (1994), 42–51.
- [15] G. R. Feijóo, A new method in inverse scattering based on the topological derivative, *Inverse Probl.*, 20 (2004), 1819–1840.
- [16] M. Hintermüller and A. Laurain, Electrical impedance tomography: from topology to shape, *Control Cybernet.*, 37 (2008), 913–933.
- [17] M. Hintermüller, A. Laurain, and A. A. Novotny, Second-order topological expansion for electrical impedance tomography, preprint.
- [18] O. Kwon, J. K. Seo, and J. R. Yoon, A real-time algorithm for the location search of discontinuous conductivities with one measurement, *Comm. Pure Appl. Math.*, 55 (2002), 1–29.
- [19] A. Malcolm and B. Guzina, On the topological sensitivity of transient acoustic fields, *Wave Motion* 45 (2008), 821–834.
- [20] M. Masmoudi, J. Pommier, and B. Samet, The topological asymptotic expansion for the Maxwell equations and some applications, *Inverse Probl.*, 21 (2005), 547–564.
- [21] G. W. Milton, *The Theory of Composites*, Cambridge Monographs on Applied and Computational Mathematics, Cambridge University Press, 2001.
- [22] J. Rocha de Faria and A. A. Novotny, On the second order topological asymptotic expansion, *Struct. Multidiscip. Optim.*, 39 (2009), 547–555.
- [23] J. Sokółowski and A. Zochowski, On the topological derivative in shape optimization, *SIAM J. Control Optim.*, 37 (1999), 1251–1272.
- [24] M. S. Vogelius and D. Volkov, Asymptotic formulas for perturbations in the electromagnetic fields due to the presence of inhomogeneities, *Math. Model. Numer. Anal.*, 34 (2000), 723–748.